ARTICLE

Growth and Electronic Properties of Ag Nanoparticles on Reduced CeO_{2-x}(111) Films

Dan-dan Kong, Yong-he Pan, Guo-dong Wang, Hai-bin Pan, Jun-fa Zhu*

National Synchrotron Radiation Laboratory, University of Science and Technology of China, Hefei 230029, China

(Dated: Received on September 28, 2012; Accepted on November 7, 2012)

Ag nanoparticles grown on reduced CeO_{2-x} thin films have been studied by X-ray photoelectron spectroscopy and resonant photoelectron spectroscopy of the valence band to understand the effect of oxygen vacancies in the CeO_{2-x} thin films on the growth and interfacial electronic properties of Ag. Ag grows as three-dimensional particles on the CeO_{2-x}(111) surface at 300 K. Compared to the fully oxidized ceria substrate surface, Ag favors the growth of smaller particles with a larger particle density on the reduced ceria substrate surface, which can be attributed to the nucleation of Ag on oxygen vacancies. The binding energy of Ag3d increases when the Ag particle size decreases, which is mainly attributed to the final-state screening. The interfacial interaction between Ag and CeO_{2-x}(111) is weak. The resonant enhancement of the 4f level of Ce^{3+} species in RPES indicates a partial Ce^{4+}→Ce^{3+} reduction after Ag deposited on reduced ceria surface. The sintering temperature of Ag on $CeO_{1.85}$(111) surface during annealing is a little higher than that of Ag on CeO_2(111) surface, indicating that Ag nanoparticles are more stable on the reduced ceria surface.

Key words: Silver, Ceria, Growth, Electronic structure, X-ray photoelectron spectroscopy, Resonant photoelectron spectroscopy

I. INTRODUCTION

In heterogeneous catalysis, Ag-on-ceria systems have been widely used in a variety of catalytic reactions, such as in NO reduction, CO and hydrocarbon oxidation [1, 2], methane oxidation [3], and formaldehyde oxidative decomposition [4]. Moreover, the use of Ag deposited on ceria was also found to increase the rate of carbon gasification in the oxidation of carbon soot particles compared to other noble metals [5−7]. To gain fundamental insight into the nature of chemistry of Ag/ceria catalysts, several surface science studies in terms of the growth, structure, and reactivity of vapor-deposited Ag nanoparticles on CeO_{2-x}(111)($0 \le x < 5$) surfaces have been performed [8−10]. Recently, we studied the growth and interfacial electronic properties of Ag on the CeO_2(111) thin films using synchrotron radiation photoemission spectroscopy [8]. A three-dimensional (3D) growth mode with a density of $\sim 1\times10^{12}$ particles/cm^2 for Ag on a well-ordered CeO_2(111) was reported. However, when the CeO_2(111) surface has a high density of defects (*i.e.*, less-ordered), an initial two-dimensional (2D) growth up to 0.3 ML due to Ag population on defect sites followed by a 3D growth with a density of $\sim 4\times10^{12}$ particles/cm^2 for Ag was observed. Farmer *et al.* also reported that Ag binds more strongly on the more reduced CeO_{2-x}(111) surfaces using microcalorimetric techniques [9], which is also consistent with the scanning tunneling microscopy (STM) studies of Ag nanoparticles grown on ceria [10], which showed surface oxygen vacancies act as nucleation centers for Ag nanoparticles.

In this work, we focus the effect of surface oxygen vacancies in the ceria films on the growth of Ag particles and the Ag-ceria interfacial electronic properties. We use resonant photoelectron spectroscopy (RPES) together with X-ray photoelectron spectroscopy (XPS) and low energy electron diffraction (LEED) to investigate the growth, nucleation, and electronic properties of Ag on the reduced CeO_{2-x}(111) thin films which were prepared *in situ* on a Ru(0001) substrate. Resonant photoemission using synchrotron radiation is one of the most sensitive tools for the detection of changes in the oxidation state of ceria [11, 12]. This method is based on determining Ce4f occupancy in the valence band spectra in the Ce4d→4f photoabsorption region [12]. Different 4f configurations for $Ce^{4+}(4f^0)$ and $Ce^{3+}(4f^1)$ result in different spectroscopic features in the valence-band (VB) spectra [13]. From the core-level binding energies and Auger parameters, the electronic properties of the Ag/CeO_2 interface with various sizes of Ag nanoparticles are determined. The thermal stability/sintering process of the Ag nanoparticles with different initial sizes at elevated temperatures is also ex-

*Author to whom correspondence should be addressed. E-mail: jfzhu@ustc.edu.cn

amined.

II. EXPERIMENTS

All the experiments were performed at the Photoemission Endstation at beamline U20 in the National Synchrotron Radiation Laboratory, Hefei, China. The detailed description of the beamline and endstation can be found in our previous work [8]. Briefly, this beamline is connected to a bending magnet and equipped with three gratings that cover photon energies from 60 eV to 1000 eV with a resolving power ($E/\Delta E$) better than 1000. The endstation consists of an analysis chamber and a sample preparation chamber, whose base pressures are 26.7 and 66.7 nPa, respectively, and a sample load-lock system. The analysis chamber is equipped with a VG Scienta R3000 electron energy analyzer, a twin anode (Mg and Al) X-ray source, rear-view LEED optics, a quadrupole mass spectrometer (Pfeiffer QMS220), and an Ar^+ sputter gun. The preparation chamber is connected with a quick load-lock port and houses an e-beam evaporator for Ce and a home-built evaporator for Ag.

The photoemission spectra were recorded at normal emission and have been normalized to the photon flux which was calibrated by measuring the Au4f spectra from a clean Au foil attached to the sample holder. Valence band spectra were recorded with a photon energy of 170 eV. Al Kα (1486.6 eV) was used to probe Ag3d and O1s core levels. All the binding energies (BEs) were calibrated with respect to the $Au4f_{7/2}$ (BE=84 eV) feature from the Au foil, which was measured immediately after each spectrum.

The Ru(0001) single crystal (10 mm diameter and 2 mm thickness) sample, purchased from MaTeck GmbH, Germany, was used as the substrate. The sample was mounted on a Mo sample holder which was fixed by Ta wires at the sides. A K-type thermocouple was used to monitor the sample temperature. The sample was cleaned by repeated cycles of Ar^+ bombardment at room temperature followed by annealing up to 1300 K until no contaminants were detected by XPS and a sharp LEED pattern was observed.

Reduced $CeO_{2-x}(111)$ thin films were prepared by evaporating cerium metal onto Ru(0001) with a constant substrate temperature of 700 K in the presence of oxygen gas followed by annealing at 980 K for 10 min [14−16]. Our previous studies have shown that the fully oxidized CeO_2 grew with an oxygen pressure of 26.6 μPa and a Ce flux of 0.003 nm/min [8]. The reduced ceria can be obtained by decreasing the oxygen pressure during the cerium evaporation. By varying the oxygen pressure, different degree of reduced ceria films can be obtained. For example, oxygen pressure of 8 μPa was used to obtain $CeO_{1.81}$ thin films. Metallic cerium (99.99%, Goodfellow) evaporated from an electron bombarded W crucible using a water-cooled e-beam evaporator that was equipped with an integral flux monitor, enabling real-time control of the deposition rate. The thickness of the $CeO_{2-x}(111)$ films is about 3−4 nm, which is similar to that of fully oxidized CeO_2 film reported previously [8]. One equivalent layer (ML) is defined as 7.89×10^{14} CeO_2 units per cm^2 with the thickness of 0.31 nm [9]. After film growth, LEED patterns were always checked to assess the long-range order of the films. CeO_{2-x} film exhibits a p(1.4×1.4) LEED pattern which are comparable to that from the fully oxidized film [17].

Ag was deposited onto the ceria films by evaporating Ag metal (99.999%, Alfa Aesar) from a tantalum basket, which was thoroughly degassed prior to use. A very slow deposition rate of Ag (0.002 ML/min) was used in our experiments. One monolayer (ML) of Ag is defined throughout as the number of Ag atoms per area in a closed-packed (111) layer of Ag atoms with lattice parameters of bulk Ag (1 ML=1.4×10^{15} atoms/cm^2), which is about twice as much as the number of oxygen atoms in $CeO_2(111)$ exposed to the vacuum per unit area [9].

III. RESULTS AND DISCUSSION

A. Growth of Ag on reduced CeO_{2-x}(111) at room temperature

It has been demonstrated that the growth mode of Ag can be affected by the roughness of the CeO_2 films and Ag preferentially populates the defect sites of the surface [8]. The growth of Ag is now studied on the reduced $CeO_{2-x}(111)$ films with different reduction degrees to further examine the effect of oxygen vacancies on the growth mode of Ag using XPS. The percentage of Ce^{3+} concentration in the CeO_{2-x} films was determined from the Ce3d XPS spectra, as described previously [8]. For example, when the partly reduced ceria film contains 30%Ce^{3+}, the film is designed to be $CeO_{1.85}$. While on the fully reduced $CeO_{1.5}$ film, only the features associated with Ce^{3+} can be observed [16, 18]. With increasing the reduction degree of ceria, the increase in the surface roughness as well as the number of surface defects have been observed in the previous STM studies [16, 19].

As seen in Fig.1, on the $CeO_2(111)$ surface the Ag signal exhibits behavior indicative of 3D island growth with an island density of $\sim10^{12}$ islands/cm^2, agreeing well with previous photoemission studies [8]. On the two reduced $CeO_{2-x}(111)$ surfaces ($CeO_{1.85}$ and $CeO_{1.5}$), the Ag signals also indicate that the growth of Ag exhibits 3D behavior. However, the best fit for the Ag signals grown on $CeO_{1.85}(111)$ surface is obtained with a larger particle density of $\sim2\times10^{12}$ islands/cm^2 in comparison with that on the well-ordered $CeO_2(111)$ surface which was postannealed at the same temperature (980 K) as those on the reduced surfaces. Further increasing the reduction degree to $CeO_{1.5}(111)$ leads

DOI:10.1088/1674-0068/25/06/713-718

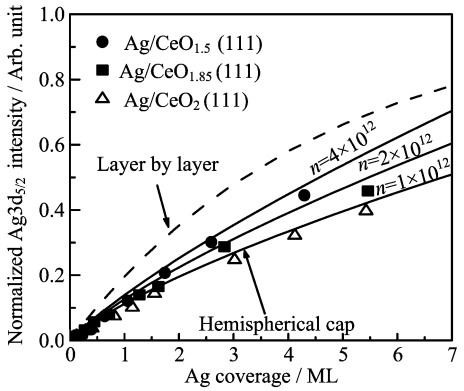

FIG. 1 Integrated $Ag3d_{5/2}$ XPS peak intensities normalized to that of bulk Ag versus coverage for Ag growth on 4 nm thick CeO_{2-x}(111) films grown on Ru(0001) at room temperature. The solid data points represent the results from the $CeO_{1.85}$(111) and $CeO_{1.5}$(111) films, respectively, while the open data points are the results obtained from the CeO_2(111) film. The dashed curves correspond to what is expected if Ag grows in a layer-by-layer growth mode, and the solid curves represent a hemispherical cap model with constant island densities of 4×10^{12} and 1×10^{12} islands/cm^2. The inelastic mean free path used for calculation is 1.54 nm for Ag, obtained from Ref.[21], and the detection angle was 45°.

to a continued increase of the Ag particles density to $\sim4\times10^{12}$ islands/cm^2. This means that at the same Ag coverage, smaller Ag particles with larger island density are formed on the reduced CeO_{2-x}(111) surface as compared to those on the CeO_2(111) surface. Moreover, the more reduced the ceria film, the smaller Ag particles on it. The increased Ag particle density on the reduced ceria can be attributed to the increase of surface oxygen vacancy defect sites which have stronger bonding to Ag [10, 20]. These results agree very well with the STM studies for Ag on the CeO_{2-x} surface [10]. However, based on AES and ISS measurements, a larger Ag particle density of $\sim4\times10^{12}$ islands/cm^2 on the reduced $CeO_{1.8}$(111)/Pt(111) surface was reported previously [9]. This discrepancy may be due to the difference in the surface structure of CeO_{2-x} film, which arises from the difference in the preparation recipe of ceria films and the substrate.

B. Interfacial electronic properties

Reduction of CeO_2(111) upon Ag deposition was observed previously using photoelectron spectroscopy [8, 10]. As a possible origin of this phenomenon, we proposed reduction of ceria caused by the reverse spillover of lattice oxygen to the surface of the supported Ag nanoparticles [8]. We used the Auger parameter method which was first introduced by Wagner [22, 23] to distinguish the initial and final state contributions to the particle size-dependent Ag3d core level shifts. In general, the initial state effects can be attributed to the electron charge transfer between the supported metal and the substrate and/or intrinsic size effects due to the reduced metal-metal coordination in the metal particles, while the final state effects arise from the final state screening, *i.e.*, relaxation effects, which depend on the shape and size of the particles as well as the supports [24−26]. Our experimental results suggested that the initial state contribution to the Ag3d core level shifts is negligible, and the observed positive shift is entirely due to the final state screening. Therefore, the Ag nanoparticles on CeO_2(111) remain metallic state. However, it should be mentioned that this finding disagrees with the theoretical study by Luches *et al.* [10], where a direct electron transfer from the Ag nanoparticles to the ceria support was claimed. The interactions between Ag nanoparticles and the reduced ceria surface are further studied to examine the effect of oxygen vacancies of ceria on the electronic properties of Ag. Here we also use the Auger parameter method to distinguish the relative contributions of the initial and final state effects on the Ag core-level binding energy shifts as a function of particle sizes. According to this method, the change of the Auger parameter (α), which is defined as sum of the kinetic energy (KE) of the Auger peak and the binding energy of the core level peak, approximately equals twice the final state contributions to the core level shifts [22, 23, 27].

In Fig.2 (a) and (b), the $Ag3d_{5/2}$ core level binding energy and Ag M_5VV Auger transition kinetic energy of Ag growth on a $CeO_{1.85}$(111) film are plotted as a function of Ag coverage at 300 K. As can be seen, with decreasing Ag coverage, the $Ag3d_{5/2}$ BE shifts to a higher BE, while the KE of the M_5VV Auger transition shifts to a lower KE. At 0.04 ML Ag coverage, with respect to the bulk Ag value, the Ag3d BE is higher by 0.6 eV and the M_5VV Auger peak position is lower by 1.5 eV. Above 10.0 ML Ag coverage, they all approach the bulk Ag value. The BE shifts of Ag with increasing Ag coverage on $CeO_{1.85}$(111) are similar to that on CeO_2(111) [8].

The Auger parameter α, calculated from the sum of the $Ag3d_{5/2}$ BE (Fig.2(a)) and the M_5VV Auger transition KE (Fig.2(b)), as a function of Ag coverage is plotted in Fig.2(c). As seen, α increases with the increasing Ag coverage from 718.9 eV at 0.04 ML to 720.0 eV for the bulk value. The contributions from the final state (ΔR) and the initial state ($\Delta\varepsilon$) to the core level BE shifts estimated from the value of $\Delta\alpha$, as described in detail previously [8], are plotted as a function of Ag coverage in Fig.2(d). It is obvious that over the entire coverage we investigated, the final state contribution to the Ag3d core level binding energy shifts is dominant. At very low coverage (0.04 ML), the final state effects contribution is calculated to be ∼0.5 eV, while the initial state contribution is −0.1 eV. Essentially initial state contribution is very small (within ±0.1 eV) from very low (0.04 ML) to high (10.0 ML) Ag coverages. These

DOI:10.1088/1674-0068/25/06/713-718

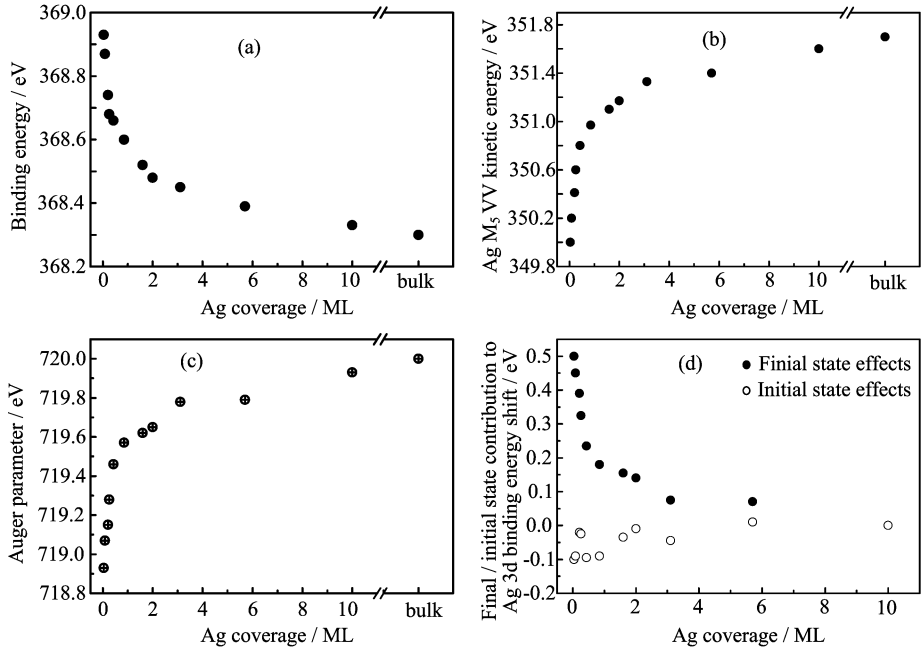

FIG. 2 (a) $Ag3d_{5/2}$ core level binding energy, (b) Ag M_5VV Auger peak kinetic energy, (c) Auger parameter, and (d) initial state and final state contributions to the core level binding energy shifts as a function of Ag coverage on $CeO_{1.85}(111)$ at 300 K. The total core level shifts come from $\Delta\varepsilon-\Delta R$, where $\Delta\varepsilon$ and ΔR represent the initial state and final state contributions, respectively.

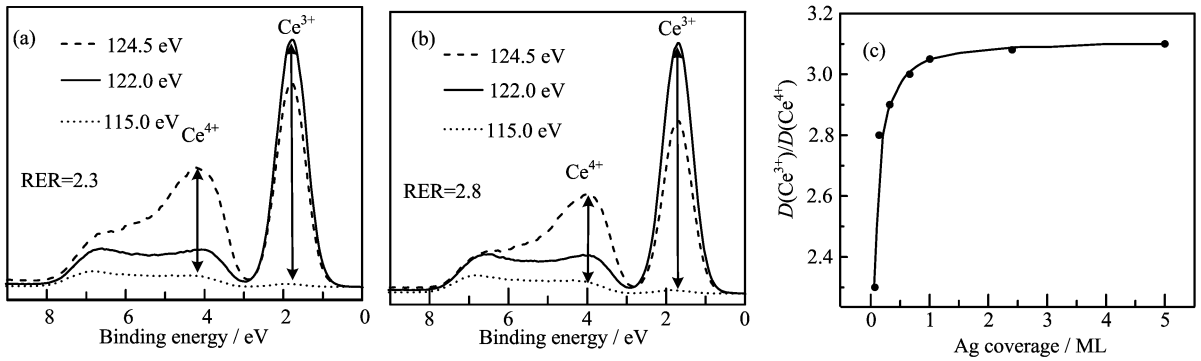

FIG. 3 Valence band photoemission spectra of (a) 4 nm clean $CeO_{1.85}(111)$, and (b) 0.07 ML Ag on $CeO_{1.85}(111)$ taken at photon energies: $h\nu$=115.0 eV (off-resonance), $h\nu$=122.0 eV (Ce^{3+} resonance), $h\nu$=124.5 eV (Ce^{4+} resonance). (c) Resonance enhancement ratio $D(Ce^{3+})/D(Ce^{4+})$ from RPES as a function of Ag coverage on the $CeO_{1.85}(111)$ film.

results indicate a relative weak interaction between Ag clusters and the reduced ceria thin film. However, since at the same coverage the 3D growth of Ag nanoparticles with larger number of island densities on the reduced ceria films compared to that on the fully oxidized ceria film suggests that the interaction of Ag with reduce ceria, in spite of the weakness, is still slightly stronger than Ag with fully oxidized ceria [8]. This is further confirmed by the higher sintering temperatures of the Ag nanoparticles on reduced ceria at a given coverage.

Changes of the oxidation state of Ce upon Ag deposition can be monitored by valence band spectra following the characteristic Ce4f photoemission feature of Ce^{3+} [8]. Thus, a primary indication of CeO_2 reduction due to Ag deposition at 300 K was observed [8]. However, in the present work, the intensity of the Ce4f peak in VB spectra is already very strong for the clean partially reduced CeO_{2-x} films. It is difficult to identify small changes in the Ce4f intensity corresponding to changes of the Ce^{3+} concentration caused by Ag deposition. Moreover, the Ag deposition even causes the damping of the Ce4f signals. Resonant photoelectron spectroscopy (RPES) has been proven to be more sensitive to the stoichiometry variations than the analysis of VB spectra and is not dependent on the absolute ceria amount and/or spectra overlapping with other peaks belonging to additive or substrates if present [11]. The RPES showed a strong dependence on the valence state with

DOI:10.1088/1674-0068/25/06/713-718

on-resonance spectra obtained near 125.0 and 122.0 eV for $4f^0$ and $4f^1$ configurations in the ground state, respectively [12]. According to the previously published results [11, 28], we can recognize two resonant features located at BEs of 4.0 and 1.6 eV that reach their maximum enhancements at $h\nu$=124.5 eV (Ce^{4+} resonance) and 122.0 eV (Ce^{3+} resonance), respectively. At the photon energy of 115.0 eV, there is no resonance for both Ce^{4+} and Ce^{3+}. The RPE spectra of the clean $CeO_{1.85}$(111) surface at photon energies of 115.0, 122.0, and 124.5 eV are shown in Fig.3(a). In Fig.3(b) the corresponding resonant spectra of 0.07 ML Ag deposited $CeO_{1.85}$(111) are shown for comparison. The resonance enhancement ratio (RER), $D(Ce^{3+})/D(Ce^{4+})$, can be calculated by dividing the two resonant maxima after subtraction of the off-resonance spectrum. For the clean $CeO_{1.85}$ film, the ratio $D(Ce^{3+})/D(Ce^{4+})$ is 2.3. Upon 0.07 ML Ag deposition, this ratio increases to 2.8. Moreover, with increasing Ag coverage, the RER further increases. As shown in Fig.3(c), the RER ratio increases rapidly at coverage up to 1 ML followed by a slower increase; it reaches the value of 3.1 at 5 ML Ag coverage. Therefore, it is clear that the $CeO_{1.85}$(111) surface is further reduced after Ag deposition. This finding is similar to that of Ag on stoichiometric CeO_2(111) [8, 10]. Since the above Auger parameter analysis shows that a very weak interaction between Ag nanoparticles and the reduced ceria thin film, the reduction of CeO_{2-x} resulting electron transfer from Ag to CeO_{2-x}(111) can be excluded. As suggested previously [8], the increase in the Ce^{3+} concentration after Ag deposition may also be ascribed to the reverse spillover of oxygen from ceria to the Ag particles.

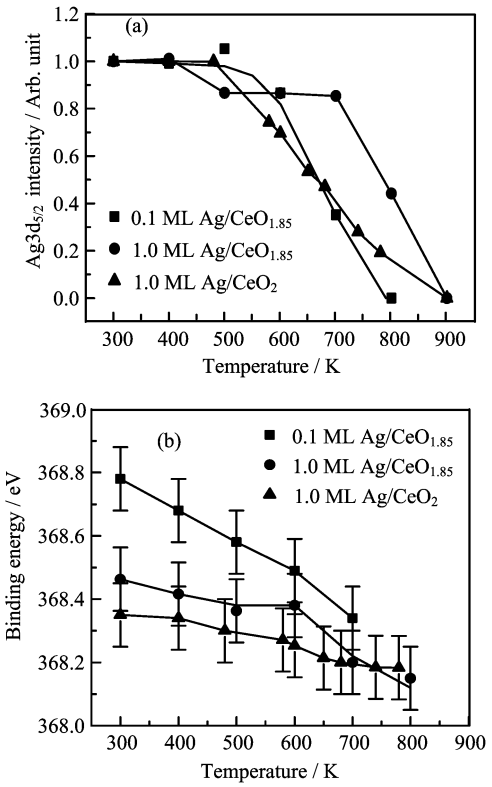

FIG. 4 (a) $Ag3d_{5/2}$ peak intensities for 0.1 and 1.0 ML Ag on $CeO_{1.85}$(111), and 1.0 ML Ag on CeO_2(111) as a function of annealing temperature. (b) Binding energies of $Ag3d_{5/2}$ spectra for 0.1 and 1.0 ML Ag on $CeO_{1.85}$(111), and 1.0 ML Ag on CeO_2(111) as a function of annealing temperature. The spectra were collected at 300 K.

C. Thermal sintering

It has been reported previously that annealing the Ag nanoparticles on fully oxidized CeO_2(111) in UHV leads to significant sintering of Ag particles before they desorb from the surface [8]. To determine the thermal stability of Ag nanoparticles on reduced CeO_{2-x}, we have carried out the following experiments: Ag deposited on $CeO_{1.85}$(111) at 300 K with two different coverages were annealed at elevated temperatures, after which Ag3d spectra were collected at 300 K. As shown in Fig.4(a), the $Ag3d_{5/2}$ peak intensities normalized to the value at 300 K are plotted as a function of temperature for 0.1 and 1.0 ML Ag on $CeO_{1.85}$(111), respectively. With increasing annealing temperature, the $Ag3d_{5/2}$ intensity for 0.1 ML Ag starts to decrease already at 600 K, while for 1.0 ML Ag the $Ag3d_{5/2}$ intensity remains nearly unchanged up to 700 K. When the temperature is higher than 700 K, the $Ag3d_{5/2}$ intensities from both surfaces decrease rapidly. At about 900 K, almost no Ag signal can be detected. According to previous studies [8], the decrease in intensity of $Ag3d_{5/2}$ spectra during annealing before 800 K can be attributed to particle sintering on the surface. Above 800 K, the sharp decrease in peak intensity is due to the Ag desorption from the surface. By 900 K, all Ag desorbs from the surface, leading to no detectable Ag signal by XPS. The sintering temperature for Ag on the reduced ceria films is found a little higher (∼100 K) than the case of the same coverage of Ag on the oxidized films. This is attributed to the oxygen vacancies on the reduced CeO_{2-x} surface which can stabilize the Ag particles through a stronger interaction between oxygen vacancies and Ag particles [9, 10, 29]. The initial sintering temperature for a low coverage Ag film (0.1 ML) is lower than that for a high coverage film (1.0 ML), indicating that larger Ag particles are more thermally stable than the smaller ones on the reduced ceria. This phenomenon is similar to what was observed for Ag on stoichiometric CeO_2(111) [8] and Au on ZrO_2(111) [30] which may be attributed to that the small Ag particles undergo sintering not only by the Ostwald ripening but also by facile diffusion on the surface and coalesce, whereas the large particles might sinter mainly through the Ostwald ripening [31]. In addition, the desorption temperature of small Ag particles is lower than that of large particles. These results are similar to those of Ag on CeO_2(111) where STM showed

DOI:10.1088/1674-0068/25/06/713-718

that the smaller Ag particles desorb more easily on the surface [10].

The Ag sintering process on $CeO_{1.85}(111)$ before desorption is further confirmed by the observation of the shifts of $Ag3d_{5/2}$ BEs as well as the changes of the full width of half-maximum (FWHM) of the $Ag3d_{5/2}$ peaks. Figure 4(b) displays the variations of $Ag3d_{5/2}$ BEs as a function of annealing temperature for 0.1 and 1.0 ML Ag on $CeO_{1.85}(111)$, respectively. Similar to the observations of Ag on $CeO_2(111)$ [8] for both Ag coverages, the BE of the $Ag3d_{5/2}$ peak shifts toward lower BE, and the FWHM (not shown) of the $Ag3d_{5/2}$ peak decreases during annealing. The changes of both BE and FWHM of $Ag3d_{5/2}$ peaks with temperature are more apparent for 0.1 ML Ag than for 1.0 ML since the initial particle size is smaller in the former case. As discussed in our previous work [8], they can be attributed to the sintering process of Ag on the $CeO_{1.85}(111)$ surface.

IV. CONCLUSION

We used RPES and XPS to investigate the growth, nucleation, and electronic properties of Ag on the reduced ceria thin films grown on Ru(0001). The results clearly indicate that Ag grows three-dimensionally on the $CeO_{2-x}(111)$ surface at 300 K. The reduced CeO_{2-x} surface has a higher defects density, which causes the formation of Ag nanoparticles with smaller particles and a higher particle density compared to those on CeO_2. Final state effects are concluded to be primarily responsible for the core level binding energy shifts of Ag deposited on $CeO_{1.85}(111)$ surface. No strong interfacial interaction between Ag and ceria is found. Nevertheless, some more Ce^{3+} states appear on the reduced ceria surface after Ag deposition. The oxygen vacancies can stabilize the adsorbed Ag nanoparticles, leading to a slightly higher sintering temperature of Ag nanoparticles on the reduced $CeO_{2-x}(111)$ surfaces.

V. ACKNOWLEDGMENTS

This work was supported by the National Natural Science Foundation of China (No.20873128), the "Hundred Talents Program" of the Chinese Academy of Sciences, the Specialized Research Fund for the Doctoral Program of Higher Education (SRFDP) of Ministry of Education (No.200803580012), and the National Basic Research Program of China (2010CB923302).

[1] P. Bera, K. C. Patil, and M. S. Hegde, Phys. Chem. Chem. Phys. **2**, 3715 (2000).
[2] S. Chang, M. Li, Q. Hua, L. Zhang, Y. Ma, B. Ye, and W. Huang, J. Catal. **293**, 195 (2012).
[3] L. Kundakovic and M. Flytzani-Stephanopoulos, J. Catal. **179**, 203 (1998).
[4] S. Imamura, D. Uchihori, K. Utani, and T. Ito, Catal. Lett. **24**, 377 (1994).
[5] E. Aneggi, J. Llorca, C. de Leitenburg, G. Dolcetti, and A. Trovarelli, Appl. Catal. B **91**, 489 (2009).
[6] L. L. Murrell and R. T. Carlin, J. Catal. **159**, 479 (1996).
[7] K. Shimizu, H. Kawachi, and A. Satsuma, Appl. Catal. B **96**, 169 (2010).
[8] D. D. Kong, G. D. Wang, Y. H. Pan, S. W. Hu, J. B. Hou, H. B. Pan, C. T. Campbell, and J. F. Zhu, J. Phys. Chem. C **115**, 6715 (2011).
[9] J. A. Farmer, J. H. Baricuatro, and C. T. Campbell, J. Phys. Chem. C **114**, 17166 (2010).
[10] P. Luches, F. Pagliuca, S. Valeri, F. Illas, G. Preda, and G. Pacchioni, J. Phys. Chem. C **116**, 1122 (2012).
[11] M. Skoda, M. Cabala, I. Matolinova, K. C. Prince, T. Skala, F. Sutara, K. Veltruska, and V. Matolin, J. Chem. Phys. **130**, 7 (2009).
[12] M. Matsumoto, K. Soda, K. Ichikawa, S. Tanaka, Y. Taguchi, K. Jouda, O. Aita, Y. Tezuka, and S. Shin, Phys. Rev. B **50**, 11340 (1994).
[13] S. Hufner, J. Phys. F **16**, L31 (1986).
[14] D. R. Mullins, P. V. Radulovic, and S. H. Overbury, Surf. Sci. **429**, 186 (1999).
[15] J. L. Lu, H. J. Gao, S. Shaikhutdinov, and H. J. Freund, Surf. Sci. **600**, 5004 (2006).
[16] Y. H. Zhou, J. M. Perket, and J. Zhou, J. Phys. Chem. C **114**, 11853 (2010).
[17] W. D. Xiao, Q. L. Guo, and E. G. Wang, Chem. Phys. Lett. **368**, 527 (2003).
[18] D. R. Mullins, S. H. Overbury, and D. R. Huntley, Surf. Sci. **409**, 307 (1998).
[19] J. L. Lu, H. J. Gao, S. Shaikhutdinov, and H. J. Freund, Catal. Lett. **114**, 8 (2007).
[20] M. Baron, O. Bondarchuk, D. Stacchiola, S. Shaikhutdinov, and H. J. Freund, J. Phys. Chem. C **113**, 6042 (2009).
[21] S. Tanuma, C. J. Powell, and D. R. Penn, Surf. Interface Anal. **17**, 911 (1991).
[22] C. D. Wagner, Anal. Chem. **44**, 967 (1972).
[23] C. D. Wagner, Anal. Chem. **47**, 1201 (1975).
[24] M. G. Mason, Phys. Rev. B **27**, 748 (1983).
[25] I. Lopez-Salido, D. C. Lim, R. Dietsche, N. Bertram, and Y. D. Kim, J. Phys. Chem. B **110**, 1128 (2006).
[26] K. Luo, X. Lai, C. W. Yi, K. A. Davis, K. K. Gath, and D. W. Goodman, J. Phys. Chem. B **109**, 4064 (2005).
[27] C. D. Wagner, L. H. Gale, and R. H. Raymond, Anal. Chem. **51**, 466 (1979).
[28] V. Matolin, V. Johanek, M. Skoda, N. Tsud, K. C. Prince, T. Skala, and I. Matolinova, Langmuir **26**, 13333 (2010).
[29] J. A. Farmer and C. T. Campbell, Science **329**, 933 (2010).
[30] Y. H. Pan, Y. Gao, G. D. Wang, D. D. Kong, L. Zhang, J. B. Hou, S. W. Hu, H. B. Pan, and J. F. Zhu, J. Phys. Chem. C **115**, 10744 (2011).
[31] X. Yu, L. S. Xu, W. H. Zhang, Z. Q. Jiang, J. F. Zhu, and W. X. Huang, Chin. J. Chem. Phys. **22**, 339 (2009).

DOI:10.1088/1674-0068/25/06/713-718